To appear in *Journal of Electronic Materials*
(Special Issue on "III-V Nitrides and SiC" March 2000)

Local electronic properties of AlGaN/GaN heterostructures probed by scanning capacitance microscopy

K. V. Smith and E. T. Yu
Department of Electrical and Computer Engineering
University of California, San Diego
La Jolla, CA 92093-0407

J. M. Redwing and K. S. Boutros
ATMI/Epitronics
21002 North 19th Avenue, Suite 5
Phoenix, AZ 85027-2726

Abstract

Local electronic properties in $Al_xGa_{1-x}N$/GaN heterostructure field-effect transistor epitaxial layer structures are probed using scanning capacitance microscopy. Acquisition of scanning capacitance images over a wide range of bias voltages combined with theoretical analysis and numerical simulation allows the presence, detailed nature, and possible structural origins of nanometer- to micron-scale inhomogeneities in electronic structure to be elucidated. Substantial lateral variations in local threshold voltages for transistor channel formation are observed, at length scales ranging from submicron to >2μm, and found to arise primarily from local variations in $Al_xGa_{1-x}N$ layer thickness. Features in electronic structure are also observed that are consistent with the existence of networks of negatively charged threading edge dislocations, as might be formed at island coalescence boundaries during epitaxial growth. The negative charge associated with these structures appears to lead to local depletion of carriers from the channel in the $Al_xGa_{1-x}N$/GaN transistor epitaxial layer structure.

I. Introduction

III-V nitride heterostructures are of outstanding current interest for a variety of device applications including blue and ultraviolet light-emitting diodes and lasers,[1] visible-blind ultraviolet photodetectors,[2,3] high-temperature/high-power electronics,[4-8] and field-emitter structures.[9,10] Although very impressive performance has been demonstrated in many such nitride-based devices, the epitaxially grown nitride semiconductor materials from which device structures are fabricated typically contain high densities of dislocations and other defects, as well as local inhomogeneities in epitaxial layer thicknesses and compositions. Because of the strong coupling between structural morphology and electronic properties that arises from the strong spontaneous and piezoelectric polarization fields in these materials, such features can give rise to pronounced local variations in electronic properties that must be characterized, understood, and controlled in nitride heterostructure materials and device engineering.

In this paper we present studies of local electronic properties in $Al_xGa_{1-x}N/GaN$ heterostructure field-effect transistor (HFET) epitaxial layer structures using scanning capacitance microscopy (SCM). This technique has been used extensively to perform dopant profiling in Si device structures,[11-13] and more recently to characterize local surface electronic structure in *n*-GaN epitaxial layers.[14] By measuring capacitance properties between a conducting proximal probe tip and the sample at a fixed tip-sample bias voltage, lateral variations in mobile carrier distributions can be observed at length scales ranging from <0.1*m*m to several *m*m. Measurement and analysis of SCM image contrast as a function of bias voltage then enables such variations to be correlated with features in structural morphology – local variations in layer thickness, compositional inhomogeneity, or extended defect structures – from which they may arise. In this manner we have observed lateral variations in $Al_xGa_{1-x}N/GaN$ HFET threshold

voltage at length scales ranging from ~0.1*m*m to >2*m*m, and determined that these are most likely to arise from local variations in $Al_xGa_{1-x}N$ epitaxial layer thickness. We have also observed features in local electronic structure that appear to correspond to island coalescence boundaries and associated threading edge dislocations or dislocation arrays within the epitaxial film[15,16] and have demonstrated that the SCM contrast observed is consistent with the presence of negative charge within these dislocation cores.

The remainder of this paper is divided into three sections. In Section II, the nitride sample structure, epitaxial growth conditions, and SCM apparatus and experimental considerations are discussed. Experimental results are presented, and discussed in the context of analytical and numerical analysis, in Section III. Section IV concludes the paper.

II. Experiment

The epitaxial layer structure used in these studies was grown by low-pressure metalorganic vapor phase epitaxy (MOVPE) on a *c*-plane (0001) sapphire substrate. Following growth of a nucleation buffer layer, 3*m*m of GaN and then 300Å of $Al_{0.25}Ga_{0.75}N$ were grown. All layers were nominally undoped, and an RMS surface roughness of 2Å was measured over a 1*m*m×1*m*m area of the final $Al_{0.25}Ga_{0.75}N$ surface. Comparable surface roughness was measured for similarly grown GaN epitaxial layers. Despite the absence of intentional doping, a two-dimensional electron gas (2DEG) forms at the $Al_xGa_{1-x}N$/GaN heterojunction interface due to the presence of a large positive electrostatic sheet charge at the interface arising from spontaneous and piezoelectric polarization.[17-20] Hall measurements performed on this structure yielded an electron concentration of ~5×10^{12} cm^{-2} and a mobility of ~1300 $cm^2/V\cdot s$ at room temperature.

A Digital Instruments 3100 scanning probe microscope system with a scanning capacitance head was used to perform atomic force microscopy (AFM) and SCM measurements on the $Al_xGa_{1-x}N$/GaN HFET structure. Imaging was performed using heavily doped p^+ Si probe tips on which ~50Å Pt was deposited by electron-beam evaporation. Electrical contact to the sample was made using conductive silver tape; we have verified that our results do not depend on whether contact is made in this manner directly to the $Al_xGa_{1-x}N$ surface, or to a fully processed Ti/Al Ohmic contact fabricated on the epitaxial layer structure. Native oxide layers present on the tip and sample surfaces served to minimize current flow during the SCM measurements. The SCM images presented here were acquired with an AC modulation of 1V and DC bias voltages ranging from –6V to 6V, and in all cases contact-mode AFM topographs were acquired simultaneously.

Figure 1 shows schematic diagrams of the $Al_xGa_{1-x}N$/GaN epitaxial layer structure, the tip-sample geometry and electrical connections used in the SCM measurements, and the electrostatic charge distribution within the probe tip and sample. As indicated in the figure, lateral resolution is achieved by scanning the probe tip across the sample surface. In addition, resolution in depth can be attained by varying the applied tip-sample DC bias voltage V_{dc}. Thus, acquisition and analysis of SCM images as a function of bias voltage allows local electronic properties to be probed with submicron to nanoscale spatial resolution in three dimensions.

Figure 2(a) shows a schematic plot of the capacitance C between the tip and HFET sample structure under investigation as a function of DC bias voltage applied to the sample, based on C-V characteristics measured for a large-area Schottky diode fabricated from the same epitaxial layer structure. Schematic energy-band-edge diagrams for the tip-sample structure are shown for each region of approximately constant capacitance. For $V_{dc}>V_{th,1}$, the 2DEG is depleted and the

capacitance is small. For $V_{th,2}<V_{dc}<V_{th,1}$, carriers are present primarily in the 2DEG and the sample capacitance measured is primarily that of the $Al_xGa_{1-x}N$ barrier. For $V_{dc}<V_{th,2}$, carriers in the sample spill over into the barrier and eventually accumulate at the $Al_xGa_{1-x}N$ surface, leading to higher values for the capacitance. In our measurements, the SCM signal is approximately proportional to dC/dV averaged over a voltage range $V_{dc}\pm V_{ac}$.[21] To obtain an approximate expression for the measured SCM signal from the *C-V* characteristic of the probe tip-sample system, we note that

$$C(V_{dc}+V_{ac}\sin wt)\approx C(V_{dc})+\left(\frac{dC}{dV}\right)_{V_{dc}}V_{ac}\sin wt\,. \qquad (1)$$

We then obtain an approximate expression for the SCM signal by computing the capacitance averaged over the AC voltage cycle in the following manner:

$$\text{SCM signal}\propto 2\int_{-1}^{1}[C(V_{dc}+V_{ac}\sin wt)-C(V_{dc})]V_{ac}\sin wt\,d(\sin wt) \qquad (2a)$$

$$\propto \frac{1}{V_{ac}}\int_{V_{dc}-V_{ac}}^{V_{dc}+V_{ac}}[C(V)-C(V_{dc})](V-V_{dc})dV \qquad (2b)$$

$$=\frac{1}{V_{ac}}\int_{V_{dc}-V_{ac}}^{V_{dc}+V_{ac}}C(V)(V-V_{dc})dV \qquad (2c)$$

The resulting SCM signal calculated for the *C-V* spectrum shown in Figure 2(a) is indicated by the solid line in Figure 2(b). In the following section we shall see that by analyzing the influence of various defect structures and of local inhomogeneities in layer thickness and composition on *C-V* characteristics, the SCM image contrast arising from such features can be predicted. Comparison of such predictions with experimentally observed SCM contrast then enables characterization of both the presence and the possible physical origins of local variations in electronic structure in the samples under investigation.

III. Results and Discussion

Contrast within the SCM images we have obtained arises from local variations in electronic structure that may be associated with defects or with local inhomogeneities in aspects of the epitaxial layer structure such as $Al_xGa_{1-x}N$ layer thickness or composition. The influence of such features on local electronic properties, and consequently on SCM image contrast, may be predicted via analytical calculations or numerical modeling. In our studies, we have used the former to analyze the influence of lateral variations in $Al_xGa_{1-x}N$ layer thickness or composition, and the latter to assess the effects of negatively charged edge threading dislocation lines, on SCM image contrast.

To determine the influence of local inhomogeneities in $Al_xGa_{1-x}N$ layer thickness or composition on SCM image contrast, we derive expressions for the dependence of $V_{th,1}$ and $V_{th,2}$ on these quantities. Following the general approach of Refs. 19 and 22, we see that the electron sheet concentration n_s at the GaN/$Al_xGa_{1-x}N$ interface is given, as a function of applied bias voltage, by

$$n_s = \left[\frac{d}{e_{\mathrm{AlGaN}}} s_{pol} + \frac{t}{e_{gap}} s_{surf} - \left(f_b - \frac{\Delta E_c - E_F}{e} \right) - V_{sample} \right] \Big/ \frac{1}{e} \left(\frac{d}{e_{\mathrm{AlGaN}}} + \frac{t}{e_{gap}} \right), \quad (3)$$

where s_{pol} is the polarization sheet charge density at the GaN/$Al_xGa_{1-x}N$ interface, s_{surf} is the sheet charge density at the $Al_xGa_{1-x}N$ surface, d is the $Al_xGa_{1-x}N$ layer thickness, t is the thickness of the insulating layer between tip and sample, e_{AlGaN} and e_{gap} are the dielectric constants of the $Al_xGa_{1-x}N$ and insulating layers, respectively, f_b is the metal-$Al_xGa_{1-x}N$ Schottky barrier height, ΔE_c is the GaN/$Al_xGa_{1-x}N$ conduction-band offset, and E_F is the Fermi energy at the GaN/$Al_xGa_{1-x}N$ interface. $V_{th,1}$, the threshold voltage (applied to the sample) for 2DEG formation, may be obtained by solving Equation (3) with $n_s = 0$, yielding

$$V_{th,1} = \frac{d}{e_{\mathrm{AlGaN}}} s_{pol} - \left(f_b - \frac{\Delta E_c - E_F}{e} \right) + \frac{t}{e_{gap}} s_{surf} . \quad (4)$$

$V_{th,2}$, the threshold voltage (applied to the sample) for spillover of carriers from the 2DEG into the barrier and towards the $Al_xGa_{1-x}N$ surface, is taken to be the voltage at which the potential drop across the $Al_xGa_{1-x}N$ barrier layer is sufficiently large that accumulation occurs at the $Al_xGa_{1-x}N$ surface, yielding

$$V_{th,2} = -f_b - \frac{t}{e_{gap}} \left[\frac{e_{\mathrm{AlGaN}}}{d} \left(\frac{\Delta E_c - E_F}{e} \right) + s_{pol} - s_{surf} \right]. \quad (5)$$

From these equations it is then possible to determine the qualitative nature of contrast, or more specifically the evolution of contrast with applied bias voltage, that will arise in the SCM images due to local variations in $Al_xGa_{1-x}N$ layer thickness and composition. In this manner it is then possible to distinguish among features in local electronic structure arising from different aspects of nanoscale structure and composition. Figure 2(b) and Figure 2(c) show SCM signal spectra calculated in the manner described above for different $Al_xGa_{1-x}N$ layer thicknesses and compositions, respectively. In each case Equations (4) and (5) were used to determine the shift in $V_{th,1}$ and $V_{th,2}$ that would be produced by a change in $Al_xGa_{1-x}N$ layer thickness or composition, and the model *C*-*V* spectra and SCM signals were derived accordingly. From Figure 2(b) we may deduce that SCM image contrast arising from a local variation in $Al_xGa_{1-x}N$ layer thickness will be inverted for $V_{dc}<V_{th,2}$ compared to that observed for $V_{dc}>V_{th,1}$. Conversely, we deduce from Figure 2(c) that SCM contrast arising from a local variation in $Al_xGa_{1-x}N$ layer composition will be qualitatively similar for $V_{dc}<V_{th,2}$ and $V_{dc}>V_{th,1}$. Thus, an analysis of the SCM image contrast obtained over a range of DC bias voltages, rather than at a single voltage, can provide insight into both the presence and the possible physical origins of local inhomogeneities in electronic structure.

Figure 3 shows 2.5*m*m×10*m*m topographic images, obtained in AFM contact mode, and corresponding SCM images of the surface of the $Al_xGa_{1-x}N$/GaN HFET structure obtained at bias voltages of –3V to 3V. The topographic images shown in the figure reveal that some thermal drift has occurred during acquisition of this image sequence. Several features observed are worthy of note. For V_{dc} = 3V, the 2DEG is depleted; the contrast observed reflects primarily the electronic structure in the GaN layer, and the paucity of features in the image is indicative of relatively uniform electronic structure at the deep submicron to micron scale. For V_{dc} = 2V to 0V, features associated with formation of the 2DEG at the GaN/$Al_xGa_{1-x}N$ interface are observed. The contrast observed in these images reflects local variations in the HFET threshold voltage. Substantial lateral variations in threshold voltage are observed, with characteristic length scales ranging from submicron to >2*m*m. Some correlation is observed between features observed in topography and those seen in SCM images within this bias voltage range. However, the systematic evolution in SCM image contrast observed as the bias voltage is varied indicates that the SCM image features represent actual local variations in electronic structure rather than topographically induced artifacts. For V_{dc} between 0V and –2V fewer features are observed, reflecting the nearly constant capacitance of the $Al_xGa_{1-x}N$ layer over this voltage range as carriers accumulate in the 2DEG.

For $V_{dc} \leq -2$V, carrier spillover into the $Al_xGa_{1-x}N$ barrier and towards the $Al_xGa_{1-x}N$ surface appears to occur. Within this range of voltages, one may clearly observe that the SCM image contrast is inverted compared to that observed for V_{dc} = 0V to 2V. Specifically, the prominent dark regions in the latter images appear bright, corresponding to a larger SCM signal, in the images obtained at more negative sample bias voltages. As noted above, this inversion of contrast is expected to occur in the presence of threshold voltage inhomogeneities arising from

local variations in $Al_xGa_{1-x}N$ layer thickness, and would not be expected if such inhomogeneities were to arise from local variations in $Al_xGa_{1-x}N$ composition. Indeed, it is not unexpected that local variations in $Al_xGa_{1-x}N$ layer thickness of a few tens of Angstroms or more might be present. Analytical calculations[23] have suggested that for a nominal $Al_xGa_{1-x}N$ layer thickness of 300Å, a variation in layer thickness of ~50Å could change n_s by ~15-20%, leading to a corresponding local variation in threshold voltage of a few to several tenths of a volt.

In addition to inhomogeneities in $Al_xGa_{1-x}N$ layer thickness that these data suggest are present in these samples, a high density of threading dislocations typically exists in epitaxially grown nitride semiconductor material. Of particular relevance to our work are studies indicating that threading edge dislocations can contain deep acceptor states[24,25] that become negatively charged in *n*-type nitride material.[14,26] Such states have been postulated to give rise to the yellow luminescence commonly observed in GaN and to lead to increased Coulomb scattering of electrons, particularly at moderate to low carrier concentrations.[26,27,28] Cathodoluminescence studies have indicated that yellow luminescence features appear to originate from extended defects, e.g., threading dislocations, as can be present at low-angle grain boundaries in epitaxially grown nitride films.[29,30] In addition, theoretical studies have indicated that local strain, and consequently polarization, fields in the vicinity of threading edge dislocations can give rise to substantial surface potential variations in GaN.[31]

We have performed numerical simulations using the Davinci three-dimensional device simulation program (Avant! Corporation) to assess the influence of charged threading edge dislocation lines on SCM image contrast. In these simulations, a single threading edge dislocation, taken to run along the [0001] direction in the crystal,[32] has been modeled as a line of acceptor states with linear density $1/c$, where c = 5.185Å is the GaN lattice parameter along the

(0001) direction.[26] A constant fractional occupation *f* has been assumed for each acceptor state, yielding a linear charge density *fe*/*c*, where *e* is the electronic charge. We have assumed a value for *f* of 0.7 in our simulations.[26] The precise value of *f*, and more generally of the linear charge density associated with a threading edge dislocation, does not significantly influence the conclusions drawn from our simulations.

The structure employed in our simulations consisted of a 300Å layer of *n*-$Al_{0.25}Ga_{0.75}N$ on 1*m*m *n*-GaN, with dopant concentrations of $1\times10^{18}cm^{-3}$ and $5\times10^{16}cm^{-3}$, respectively. An insulating oxide layer 20Å in thickness was assumed to be present atop the $Al_{0.25}Ga_{0.75}N$. A conduction-band offset of 0.5eV was assumed for the $Al_{0.25}Ga_{0.75}N$/GaN interface, and the Fermi level at the $Al_{0.25}Ga_{0.75}N$ surface was assumed to be unpinned. A polarization charge density of $+7\times10^{12}$ e/cm^2, which would yield the sheet concentration observed in large-area *C*-*V* measurements performed on these samples, was assumed to be present at the $Al_{0.25}Ga_{0.75}N$/GaN interface. A single threading edge dislocation was included, as described above, in the structure simulated. The probe tip was represented by a 200Å×200Å metal contact on the insulating oxide layer. While this relatively simple model does not include detailed effects such as the shape of the probe tip, electronic structure of the $Al_{0.25}Ga_{0.75}N$ surface, and variable occupation of acceptor states within the threading edge dislocation core, it is adequate to describe the principal effects of a negatively charged dislocation line on carrier distributions and, consequently, on the capacitance between a sample and probe tip.

Figure 4(a) shows the electron distribution obtained from our simulations within a cross-sectional plane containing the dislocation core, and with the tip located directly above the dislocation core. Results are shown for bias voltages ranging from –6V to 6V, with the voltages indicated in the figure applied to the sample relative to the tip. Several features may be noted in

the figure. A high density of electrons is present in the 2DEG at the $Al_xGa_{1-x}N$/GaN interface except in the immediate vicinity of the dislocation core. In the absence of the negative charge assumed to be present within the dislocation core, the positive polarization sheet charge at the $Al_xGa_{1-x}N$/GaN interface leads to formation of a 2DEG with a high electron density. In the immediate vicinity of the threading dislocation line, however, the large negative charge density leads to localized depletion of the 2DEG. For increasing tip-sample bias voltages, we observe that electrons begin to accumulate at the $Al_xGa_{1-x}N$ surface immediately below the probe tip. Even for large bias voltages, however, the 2DEG remains depleted in the vicinity of the dislocation core.

From the electron distributions plotted in Figure 4(a) we may deduce that the tip-sample *C*-*V* characteristic will be significantly altered when the tip is in the immediate vicinity of a threading edge dislocation. Figure 4(b) shows schematic plots of tip-sample *C*-*V* characteristics far away from a dislocation core (solid line), and in the immediate vicinity of a negatively charged dislocation core (dashed line). In the vicinity of the dislocation, the 2DEG is depleted for large positive sample voltages and the capacitance is therefore very small. As the sample voltage is reduced, a transition occurs directly from this regime to that in which electrons accumulate at the $Al_xGa_{1-x}N$ surface, for which the tip-sample capacitance is large. In the absence of the negatively charged dislocation core, there is a regime of intermediate capacitance in which carriers accumulate at the $Al_xGa_{1-x}N$/GaN interface. The corresponding SCM signals for the *C*-*V* characteristics shown in Figure 4(b), calculated in the manner described in Section II, are shown in Figure 4(c). From this figure we deduce that contrast inversion will occur in the vicinity of a threading edge dislocation as the DC sample bias voltage is varied from positive to negative values: in the vicinity of a threading edge dislocation, an SCM signal smaller than that

in the surrounding area should be observed at bias voltages V_{dc} between $V_{th,1}$ and $V_{th,2}$; at bias voltages $V_{dc}<V_{th,2}$, the SCM signal in the vicinity of a threading edge dislocation should be brighter than that in the surrounding area.

Figure 5 shows 10*m*m×10*m*m topographic and SCM images of the $Al_{0.25}Ga_{0.75}N$/GaN HFET sample structure. The RMS surface roughness in Figure 5(a), computed over a 1*m*m×1*m*m area, was 2Å. As in the SCM images shown in Figure 3, we see in Figure 5(b)-(f) a region approximately 2*m*m in diameter, marked by an "**X**", which exhibits the contrast inversion characteristic of $Al_xGa_{1-x}N$ layer thickness variations. The contrast observed in this series of images suggests that the $Al_xGa_{1-x}N$ layer is slightly thicker in this region; in the topographic image of Figure 5(a) this region in fact exhibits slightly elevated topography compared to the surrounding areas.

Also apparent in Figure 5(b)-(f) are contrast features that exhibit the behavior expected for negatively charged extended defects, e.g., arrays of threading edge dislocations. In Figure 5(b), carriers have begun to accumulate at the $Al_xGa_{1-x}N$/GaN interface to form a 2DEG; however, a network of slightly dark features, indicated by arrows, is visible, corresponding to localized regions in which the 2DEG remains depleted. In Figure 5(c)-(e), these regions exhibit contrast inversion, becoming bright relative to the surrounding areas, and becoming increasingly prominent with decreasing sample bias voltage. At V_{dc} = –5V, the contrast inversion is maintained, but becomes slightly less prominent than at –3V. This behavior is also consistent with that expected on the basis of our simulations. The network of extended defects revealed in this manner delineates regions of material with a typical diameter of ~1*m*m to several *m*m. These results indicate that extended defects structures present in epitaxially grown nitride films can give rise to pronounced local variations in electronic structure, and specifically provide evidence

that threading edge dislocations, expected to be present at island coalescence boundaries,[15] contain negative charge that can lead to local depletion of carriers in the 2DEG in an $Al_xGa_{1-x}N$/GaN HFET structure.

Also visible in Figure 5(b) are several dark features, approximately 1*m*m in diameter, that exhibit contrast inversion at negative sample bias voltages. The morphological origin of these features in electronic structure has not been determined. We note, however, that these features are each located on the network of extended defects described above, suggesting that these features may correspond to extended defects as well.

IV. Conclusions

We have used scanning capacitance microscopy to characterize nanometer- to micron-scale variations in electronic structure in an $Al_xGa_{1-x}N$/GaN HFET epitaxial layer structure. Our observations reveal that a variety of localized variations in electronic structure, arising from both variations in epitaxial film parameters such as layer thickness as well as extended defects such as threading edge dislocations, are present in epitaxially grown nitride films. By combining SCM imaging over a wide range of bias voltages with theoretical analysis and numerical simulation of electrostatic behavior in nitride heterostructures, we have been able to elucidate the existence and nature of local variations in electronic structure in the samples under investigation, as well as the features in structural morphology from which these variations are most likely to arise. Substantial lateral variations in HFET threshold voltage, at length scales ranging from submicron to >2*m*m, are observed; these appear to arise primarily from local variations in $Al_xGa_{1-x}N$ layer thickness. Local variations in electronic structure that appear to be associated with networks of extended defects are also observed. Numerical simulations indicate that these correspond to

negative charge located within arrays of threading edge dislocations, as might be formed at island coalescence boundaries during epitaxial growth. The SCM contrast observed indicates that such morphological features can lead to local depletion of carriers in the channel of the $Al_xGa_{1-x}N$/GaN HFET structure, with potentially significant consequences for performance of devices fabricated from epitaxial layers containing such defects.

The authors would like to acknowledge encouragement and technical assistance from Dr. H. Walker and W. McNeil of Dynamics Research Corporation. Part of this work was supported by BMDO (Dr. Kepi Wu). E.T.Y. would like to acknowledge financial support from the Alfred P. Sloan Research Foundation.

References

[1] S. Nakamura and G. Fasol, *The Blue Laser Diode: GaN Based Light Emitters and Lasers* (Springer-Verlag, Berlin, 1997).

[2] J. M. Van Hove, R. Hickman, J. J. Klaassen, P. P. Chow, and P. P. Ruden, *Appl. Phys. Lett.* **70**, 2282 (1997).

[3] Q. Chen, J. W. Yang, A. Osinsky, S. Gangyopadhyay, B. Lim, M. Z. Anwar, M. A. Khan, D. Kuksenkov, and H. Temkin, *Appl. Phys. Lett.* **70**, 2277 (1997).

[4] M. A. Khan, Q. Chen, M. S. Shur, B. T. McDermott, J. A. Higgins, J. Burm, W. J. Schaff, and L. F. Eastman, *IEEE Electron Device Lett.* **17**, 584 (1996).

[5] O. Aktas, Z. F. Fan, A. Botchkarev, S. N. Mohammad, M. Roth, T. Jenkins, L. Kehias, and H. Morkoç, *IEEE Electron Device Lett.* **18**, 293 (1997).

[6] Y. F. Wu, B. P. Keller, S. Keller, D. Kapolnek, P. Kozodoy, S. P. DenBaars, and U. K. Mishra, *Appl. Phys. Lett.* **69**, 1438 (1996).

[7] G. J. Sullivan, M. Y. Chen, J. A. Higgins, J. W. Yang, Q. Chen, R. L. Pierson, and B. T. McDermott, *IEEE Electron Device Lett.* **19**, 198 (1998).

[8] S. C. Binari, J. M. Redwing, G. Kelner, and W. Kruppa, *Electron. Lett.* **33**, 242 (1997).

[9] R. D. Underwood, S. Keller, U. K. Mishra, D. Kapolnek, B. P. Keller, and S. P. DenBaars, *J. Vac. Sci. Technol. B* **16**, 822 (1998).

[10] T. Kozawa, M. Suzuki, Y. Taga, Y. Gotoh, and J. Ishikawa, *J. Vac. Sci. Technol. B* **16**, 833 (1998).

[11] C. C. Williams, J. Slinkman, W. P. Hough, and H. K. Wickramasinghe, *Appl. Phys. Lett.* **55**, 1662 (1989).

[12] D. W. Abraham, C. Williams, J. Slinkman, and H. K. Wickramasinghe, *J. Vac. Sci. Technol. B* **9**, 703 (1991).

[13] C. J. Kang, C. K. Kim, J. D. Lera, Y. Kuk, K. M. Mang, J. G. Lee, K. S. Suh, and C. C. Williams, *Appl. Phys. Lett.* **71**, 1546 (1997).

[14] P. J. Hansen, Y. E. Strausser, A. N. Erickson, E. J. Tarsa, P. Kozodoy, E. G. Brazel, J. P. Ibbetson, U. Mishra, V. Narayanamurti, S. P. DenBaars, and J. S. Speck, *Appl. Phys. Lett.* **72**, 2247 (1998).

[15] X. H. Wu, P. Fini, E. J. Tarsa, B. Heying, S. Keller, U. K. Mishra, S. P. DenBaars, and J. S. Speck, *J. Cryst. Growth* **189/190**, 231 (1998).

[16] P. Fini, X. Wu, E. J. Tarsa, Y. Golan, V. Srikant, S. Keller, S. P. DenBaars, and J. S. Speck, *Jpn. J. Appl. Phys. Pt. 1* **37**, 4460 (1998).

[17] A. Bykhovski, B. Gelmont, and M. S. Shur, *J. Appl. Phys.* **74**, 6734 (1993).

[18] P. M. Asbeck, E. T. Yu, S. S. Lau, G. J. Sullivan, J. Van Hove, and J. M. Redwing, *Electron. Lett.* **33**, 1230 (1997).

[19] E. T. Yu, G. J. Sullivan, P. M. Asbeck, C. D. Wang, D. Qiao, and S. S. Lau, *Appl. Phys. Lett.* **71**, 2794 (1997).

[20] R. Gaska, J. W. Yang, A. D. Bykhovski, M. S. Shur, V. V. Kaminski, and S. M. Soloviov, *Appl. Phys. Lett.* **72**, 64 (1998).

[21] Digital Instruments Support Note No. 224, Rev. D (1999).

[22] E. T. Yu, X. Z. Dang, L. S. Yu, D. Qiao, P. M. Asbeck, S. S. Lau, G. J. Sullivan, K. S. Boutros, and J. M. Redwing, *Appl. Phys. Lett.* **73**, 1880 (1998).

[23] E. T. Yu, P. M. Asbeck, S. S. Lau, and G. J. Sullivan, *Electrochem. Soc. Proc.* **98-2**, 468 (1998).

[24] J. Elsner, R. Jones, M. I. Heggie, P. K. Sitch, M. Haugk, Th. Frauenheim, S. Oberg, and P. R. Briddon, *Phys. Rev. B* **58**, 12571 (1998).

[25] A. F. Wright and U. Grossner, *Appl. Phys. Lett.* **73**, 2751 (1998).

[26] N. G. Weimann, L. F. Eastman, D. Doppalapudi, H. M. Ng, and T. D. Moustakas, *J. Appl. Phys.* **83**, 3656 (1998).

[27] H. M. Ng, D. Doppalapudi, T. D. Moustakas, N. G. Weimann, and L. F. Eastman, *Appl. Phys. Lett.* **73**, 821 (1998).

[28] D. C. Look and J. R. Sizelove, *Phys. Rev. Lett.* **82**, 1237 (1999).

[29] F. A. Ponce, D. P. Bour, W. Götz, and P. J. Wright, *Appl. Phys. Lett.* **68**, 57 (1996).

[30] S. J. Rosner, E. C. Carr, M. J. Ludowise, G. Girolami, and H. I. Erikson, *Appl. Phys. Lett.* **70**, 420 (1997).

[31] C. C. Shi, P. M. Asbeck, and E. T. Yu, *Appl. Phys. Lett.* **74**, 573 (1999).

[32] X. H. Wu, L. M. Brown, D. Kapolnek, S. Keller, B. Keller, S. P. DenBaars, and J. S. Speck, *J. Appl. Phys.* **80**, 3228 (1996).

Figure Captions

Figure 1. (a) Schematic diagram of $Al_{0.25}Ga_{0.75}N$/GaN HFET sample structure showing probe-tip sample geometry and electrical connections for SCM measurement. (b) Schematic diagram of polarization-induced and free-carrier charge distribution.

Figure 2. (a) Model *C*-*V* spectrum for an $Al_xGa_{1-x}N$/GaN HFET structure and conducting probe tip. Threshold voltages for 2DEG formation ($V_{th,1}$) and carrier spillover into the $Al_xGa_{1-x}N$ barrier ($V_{th,2}$) and schematic energy-band diagrams for each constant capacitance region are indicated. SCM signal spectra computed from model *C*-*V* spectra for HFET structures with variations in (b) $Al_xGa_{1-x}N$ layer thickness and (c) Al concentration within the $Al_xGa_{1-x}N$ layer. Comparison of contrast at voltages indicated by arrows allows effects of local variations in layer thickness and in composition to be distinguished from each other.

Figure 3. (a) AFM topographic images and (b) simultaneously obtained SCM images of the $Al_{0.25}Ga_{0.75}N$/GaN HFET structure. The dc bias voltage applied to the sample (tip grounded) is indicated for each SCM image.

Figure 4. (a) Plot of electron distribution within an $Al_{0.25}Ga_{0.75}N$/GaN HFET structure in the vicinity of a negatively charged threading dislocation, obtained as a function of sample-to-tip dc bias voltage via three-dimensional numerical simulation. (b) Schematic model C-V spectra and (c) calculated SCM signal spectra for the HFET structure away from the threading dislocation core (solid line) and in the vicinity of the dislocation (dashed line).

Figure 5. (a) Topographic and (b)-(f) SCM images of the $Al_{0.25}Ga_{0.75}N$/GaN HFET structure. Sample bias voltages are indicated for each SCM image. Contrast in the region marked with an "**x**" is attributed to local variation in $Al_{0.25}Ga_{0.75}N$ layer thickness. Regions of contrast attributed to a network of negatively charged extended defects are indicated by arrows.

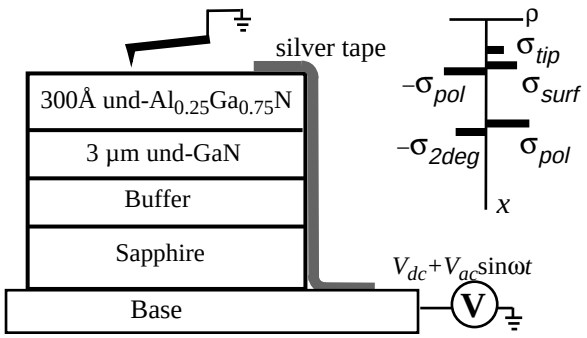

Figure 1: K. V. Smith, etal.

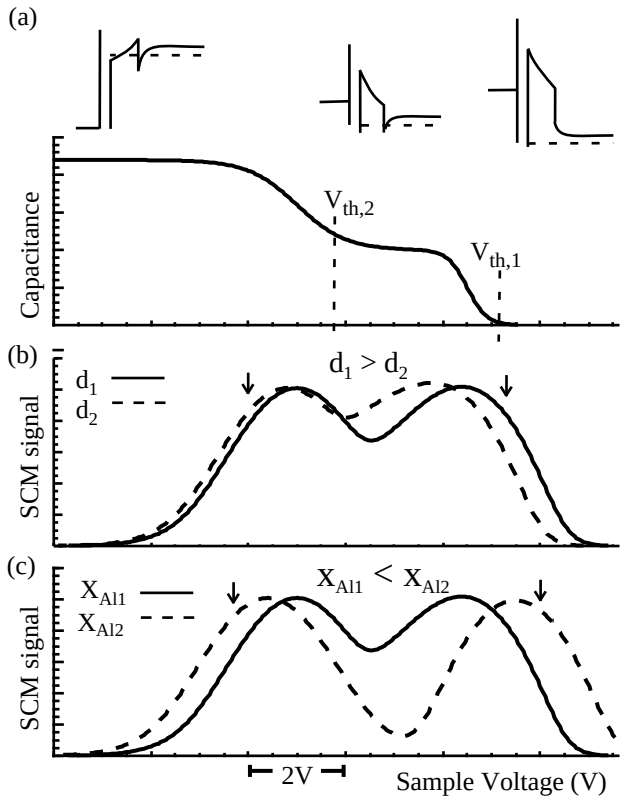

Figure 2: K. V. Smith, etal.

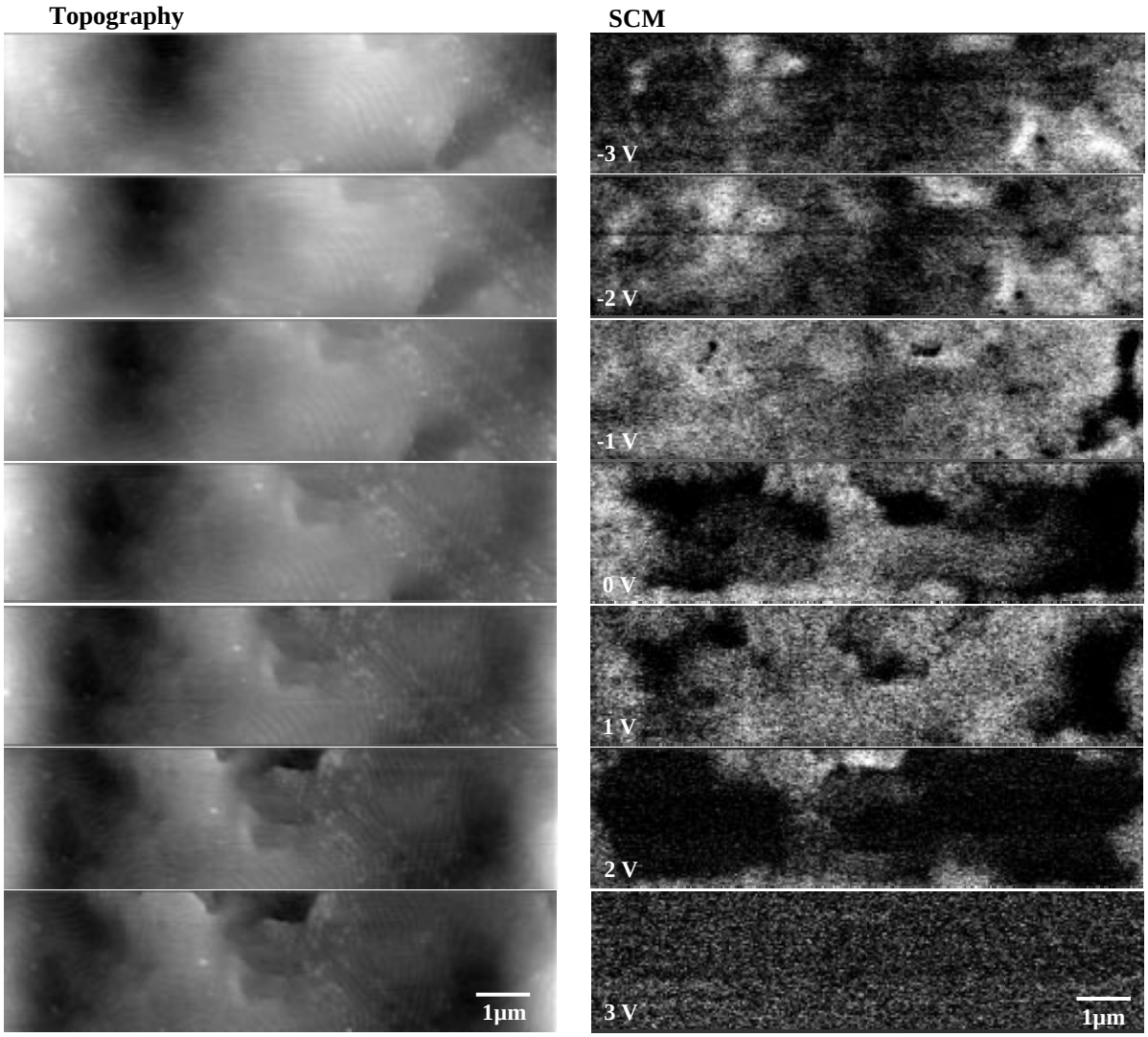

Figure 3: K. V. Smith, etal.

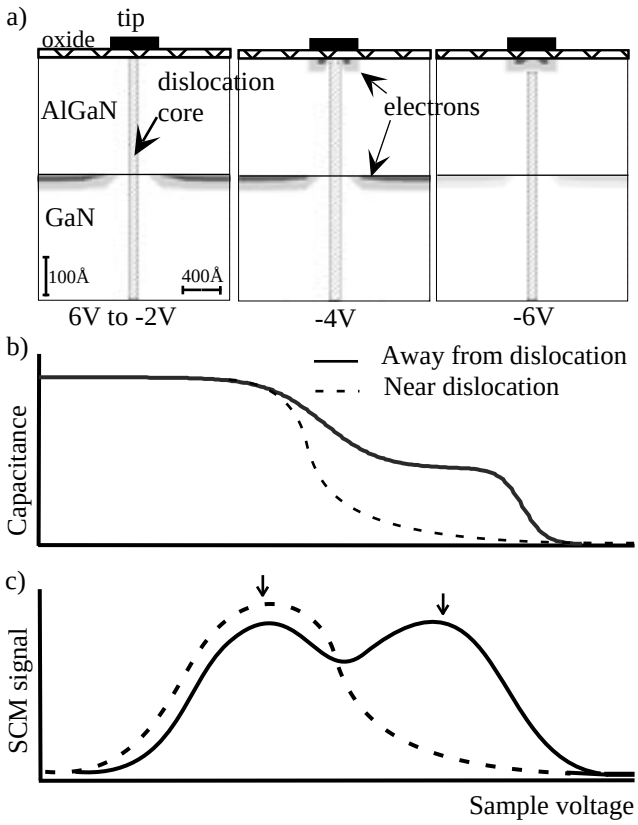

Figure 4: K. V. Smith, etal.

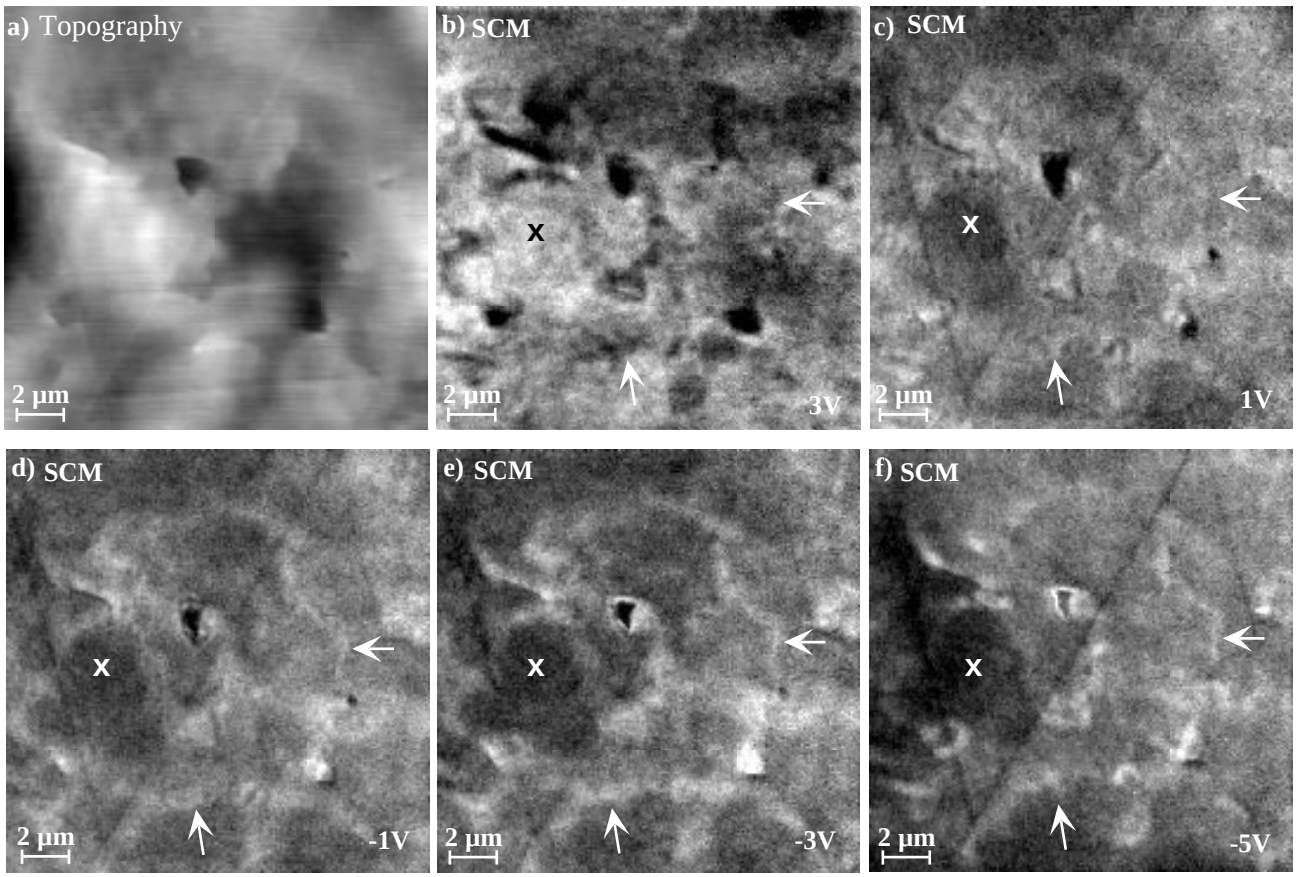

Figure 5: K. V. Smith, etal.